Composite Structures 128 (2015) 274–283

Contents lists available at ScienceDirect

Composite Structures

journal homepage: www.elsevier.com/locate/compstruct

Enhanced stiffness, strength and energy absorption for co-continuous composites with liquid filler

Yilun Liu [a], Lifeng Wang [b,*]

[a] International Center for Applied Mechanics, SV Lab, School of Aerospace, Xi'an Jiaotong University, Xi'an 710049, China
[b] Department of Mechanical Engineering, Stony Brook University, Stony Brook, NY 11794, USA

ARTICLE INFO

Article history:
Available online 28 March 2015

Keywords:
Co-continuous composites
Liquid filler
Mechanical properties
EAMS

ABSTRACT

In this work the quasi-static compressive behaviors of the co-continuous glassy polymer/liquid composites are studied. Due to the presence of liquid filler, the stiffness, yield strength and energy absorption of co-continuous composites are significantly enhanced, which comes from the additional support of liquid filler and the lateral expansion of the glassy polymer. The influence of different volume fraction of liquid filler from 0.4 to 0.7 and different geometric structures of the glassy polymer, namely simple cubic (SC) lattice, face-centered-cubic (FCC) lattice, and body-centered-cubic (BCC) lattice, is investigated. Here, SC lattice structure is the most stretch-dominated structure during compression which has the highest stiffness, yield strength, and energy absorption. A general power law can be used to describe the relations of effective elastic modulus, yield strength, and energy absorption to the volume fraction of glassy polymer, which shows almost the same power indices for the same geometric structure. These results provide guidelines for engineering and tailoring the nonlinear mechanical behavior and energy absorption of co-continuous composites for a wide range of applications and further creating multifunctional materials.

1. Introduction

Energy absorption materials and structures (EAMS) are widely used to protect persons and structures from external impulsive loads such as impacting, blasting and ballistic bullets in automotive, sporting and defense applications. Developing high performance EAMS has attracted extensive research interest to both scientists and engineers in recent years [1–6]. Two-component co-continuous structures, widely existing in biological materials (nacre, bone, exoskeleton, etc.) and manmade materials (co-continuous composite materials of block copolymers, bio-inspired clay/polymer hybrid materials, graphene-derived materials, etc.), are employed as good candidates of EAMS [7–11]. The two-component co-continuous structures are usually comprised of hard and soft phases, which can provide outstanding combinations of properties including stiffness, strength, toughness, impact resistance, and energy dissipation by combining advantages of both hard and soft materials [7,10,12]. Furthermore, the mechanical and physical properties of two-component ordered structures can be precisely adjusted by geometrical and topological arrangements of the constituents, which provide routines to engineer the macroscale properties based on the requirements of specific applications.

At present, various technologies, such as block copolymer chemistry, 3D printing, and lithography, are able to precisely fabricate ordered microstructured materials over a wide range of length scales [1,12,13]. As reported in our previous work, the co-continuous composites of glassy polymer/rubbery polymer materials with sub-millimeter feature size can be fabricated through 3D printing, which have shown excellent mechanical properties of stiffness, strength and energy dissipation [12]. The rubbery polymer is relative soft, but volumetrically incompressible, which plays as elastic filler to enhance the load capacity of glassy polymer framework. Meanwhile, the compressibility of the hybrid materials is not weakened. Although the rubbery polymer is a good filler to improve the performance of porous structures, the energy absorption of rubbery polymer itself is small and the interface binding strength between glassy polymer and rubbery polymer should be strong enough to make sure the deformation compatibility of the two components. Recently, nanoporous materials functionalized (NMF) liquid has shown impressive energy absorption ability, up to 140 J/g, which is about fifty times higher than the commercial metal foams [14–16]. Besides, for some special applications of EAMS, such as desert body armor, protective clothing for firefighting, outdoor sporting protective equipment, and protective

* Corresponding author.
E-mail addresses: yilunliu@mail.xjtu.edu.cn (Y. Liu), Lifeng.wang@stonybrook.edu (L. Wang).

http://dx.doi.org/10.1016/j.compstruct.2015.03.064
0263-8223/

structures for power battery, heat dissipation is usually required [17–19]. Therefore, the liquid cooling systems or phase-change materials should be integrated into the protective structures to conduct or absorb the thermal loads. However, the protective structures filled with liquid systems have rarely been studied in the literature.

In this paper, the compressive behaviors of co-continuous glassy polymer/liquid composites are systemically investigated. The interface between the glassy polymer and the liquid are close to those of triply periodic minimal surfaces. These structures have been found in a few material systems, such as block copolymers, micellar materials, nanocomposites, and biological exoskeletons [13,20–22]. Theoretical studies have shown theses structured materials have optimal simultaneous thermal and electrical conductivity as well as optimal multi-functional properties such as a combination of high bulk modulus together with high electrical (or thermal) conductivity, so that they have attracted a great research interest to physical scientists, material scientists, and biologists [23,24]. In Section 2, the enhancement mechanism by the liquid filler will be explored through a theoretical analysis on a simple cross-shaped structure. Then, three lattice structures with triply periodic minimal surfaces have been constructed for finite element method (FEM) simulation, which are simple cubic (SC) lattice, face-centered-cubic (FCC) lattice, and body-centered-cubic (BCC) lattice. Furthermore, the quasi-static compressive behaviors of the three lattice structures have been studied via FEM simulation, and the enhancement of stiffness, yield strength and energy abosption by the liquid filler has been analyzed in Section 3. Moreover, the discussions of possible failure mechanisms of the co-continuous glassy polymer/liquid composites are presented in Section 4, followed by conclusions in Section 5.

2. Co-continuous glassy polymer/liquid composites

Due to liquid filler, the mechanical performance of co-continuous glassy polymer/liquid composites will be significantly enhanced, which comes from the additional support of the liquid filler and the lateral expansion of the glassy polymer structures. In this section we will first explore the enhancement mechanism of the liquid filler for a simple structure of three dimensionally cross-shaped structure, as shown in Fig. 1. Thereafter, three type lattice structures with triply periodic minimal surfaces are constructed for further FEM simulations.

2.1. Theoretical analysis of the enhancement by liquid filler

The compressive behaviors of three dimensionally cross-shaped structure with liquid filler are explored. The surrounding of the co-continuous composites is sealed to construct the energy absorption system, as shown in Fig. 1(a). Here, the cross-shaped structure is consisted of three orthogonal bars, where the cross section of the bar is square with size a and the distance between neighboring intersection points is l. By considering the periodic nature of the co-continuous composites, the compressive deformation of one unit cell is studied in this work. Due to the force equilibrium of the unit cell in x and z direction, the stresses in the ligaments on the surfaces of the unit cell are $\sigma_x = \sigma_z = (A_L/A_S)P$, where P is the pressure in the liquid, $A_S = a^2$ is the cross section area of the ligaments on the surface and $A_L = l^2 - a^2$ is the cross section area of the liquid on the surface, see Fig. 1(b). Generally, the stress distribution in the cross-shaped structure can be separated into three regions, that are the intersectional region (region III), the vertical uncrossed region (region I) and the lateral uncrossed region (region II), as shown in Fig. 1(c). In this work we aim to explore the enhancement mechanism of the liquid filler, and for the simplicity of theoretical analysis, the stress distributions in the three regions are assumed homogeneous, respectively. Based on the assumption, the stresses in region I are σ_{Ix}, σ_{Iy}, σ_{Iz}, in region II are σ_{IIx}, σ_{IIy}, σ_{IIz}, and in region III are σ_{IIIx}, σ_{IIIy}, σ_{IIIz}, where $\sigma_{Ix} = \sigma_{Iz} = -P$, $\sigma_{IIy} = \sigma_{IIz} = -P$, $\sigma_{IIx} = (A_L/A_S)P$ and $\sigma_{IIIy} = \sigma_{Iy}$, $\sigma_{IIIx} = \sigma_{IIIz} = (A_L/A_S)P$. During compression, the pressure P in the liquid is positive, and thus σ_{IIx} is also positive which will cause lateral expansion of the unit cell. According to the stresses in the three regions, we can obtain the strains in the three regions as

Region I

$$\begin{aligned}\varepsilon_{Ix} &= \varepsilon_{Iz} = \frac{1}{E}\left[-P - \nu(\sigma_{Iy} - P)\right],\\ \varepsilon_{Iy} &= \frac{1}{E}(\sigma_{Iy} + 2\nu P),\end{aligned} \tag{1a}$$

Region II

$$\begin{aligned}\varepsilon_{IIx} &= \frac{1}{E}\left(\frac{A_L}{A_S}P + 2\nu P\right),\\ \varepsilon_{IIy} &= \varepsilon_{IIz} = \frac{1}{E}\left[-P - \nu\left(\frac{A_L}{A_S} - 1\right)P\right],\end{aligned} \tag{1b}$$

Region III

$$\begin{aligned}\varepsilon_{IIIx} &= \varepsilon_{IIIz} = \frac{1}{E}\left[\frac{A_L}{A_S}P - \nu\left(\sigma_{Iy} + \frac{A_L}{A_S}P\right)\right],\\ \varepsilon_{IIIy} &= \frac{1}{E}\left(\sigma_{Iy} - 2\nu\frac{A_L}{A_S}P\right),\end{aligned} \tag{1c}$$

where E and ν are Young's modulus and Poisson ratio of the solid material. The volume change of the unit cell is

$$\Delta V = l_x l_y l_z - l^3, \tag{2}$$

where, $l_y = [(1+\varepsilon_{Iy})(l-a) + (1+\varepsilon_{IIIy})a]$, $l_x = l_z = [(1+\varepsilon_{IIx})(l-a) + (1+\varepsilon_{IIIx})a]$. Substituting Eqs. (1a)–(1c) into Eq. (2), the volume change of the unit cell is

$$\Delta V = \frac{1}{E}\left[\sigma_{Iy}\left(1 - 2\nu\frac{a}{l}\right) + 2\frac{A_L}{A_S}P\left(1 - 2\nu\frac{a}{l}\right) + 6\nu P\left(1 - \frac{a}{l}\right)\right]l^3, \tag{3}$$

while the volume change of the solid is

$$\begin{aligned}\Delta V_S &= 2\Delta V_I + 4\Delta V_{II} + \Delta V_{III}\\ &= (\varepsilon_{Ix} + \varepsilon_{Iy} + \varepsilon_{Iz})(l-a)a^2 + 2(\varepsilon_{IIx} + \varepsilon_{IIy} + \varepsilon_{IIz})(l-a)a^2\\ &\quad + (\varepsilon_{IIIx} + \varepsilon_{IIIy} + \varepsilon_{IIIz})a^3\\ &= \frac{\sigma_{Iy}}{E}la^2(1-2\nu) + \frac{P}{E}\left(-6 + 12\nu + 2\frac{A_L}{A_S} - 4\nu\frac{A_L}{A_S}\right)la^2\\ &\quad - \frac{P}{E}(-6 + 12\nu)a^3.\end{aligned} \tag{4}$$

Then, the volume strain of the liquid is

$$\varepsilon_{VL} = (\Delta V - \Delta V_S)/V_L = \frac{\sigma_{Iy}}{E}k_1 + \frac{P}{E}(k_2 + k_3), \tag{5}$$

where $k_1 = \frac{l^2(l-2\nu a) - la^2(1-2\nu)}{l^3 - 3la^2 + 2a^3}$, $k_2 = \frac{A_L}{A_S}\frac{(2l-4\nu a)l^2 - (2-4\nu)la^2}{l^3 - 3la^2 + 2a^3}$ and $k_3 = \frac{(l-a)6\nu l^2 - (-6+12\nu)(la^2 - a^3)}{l^3 - 3la^2 + 2a^3}$. Therefore, the pressure in the liquid is

$$P = -K\varepsilon_{VL}, \tag{6}$$

where K is bulk modulus of the liquid. Substituting Eq. (5) into Eq. (6), we get the relation between pressure P and σ_{Iy} is

$$P = -\frac{\sigma_{Iy}k_1}{k_2 + k_3 + \frac{E}{K}}. \tag{7}$$

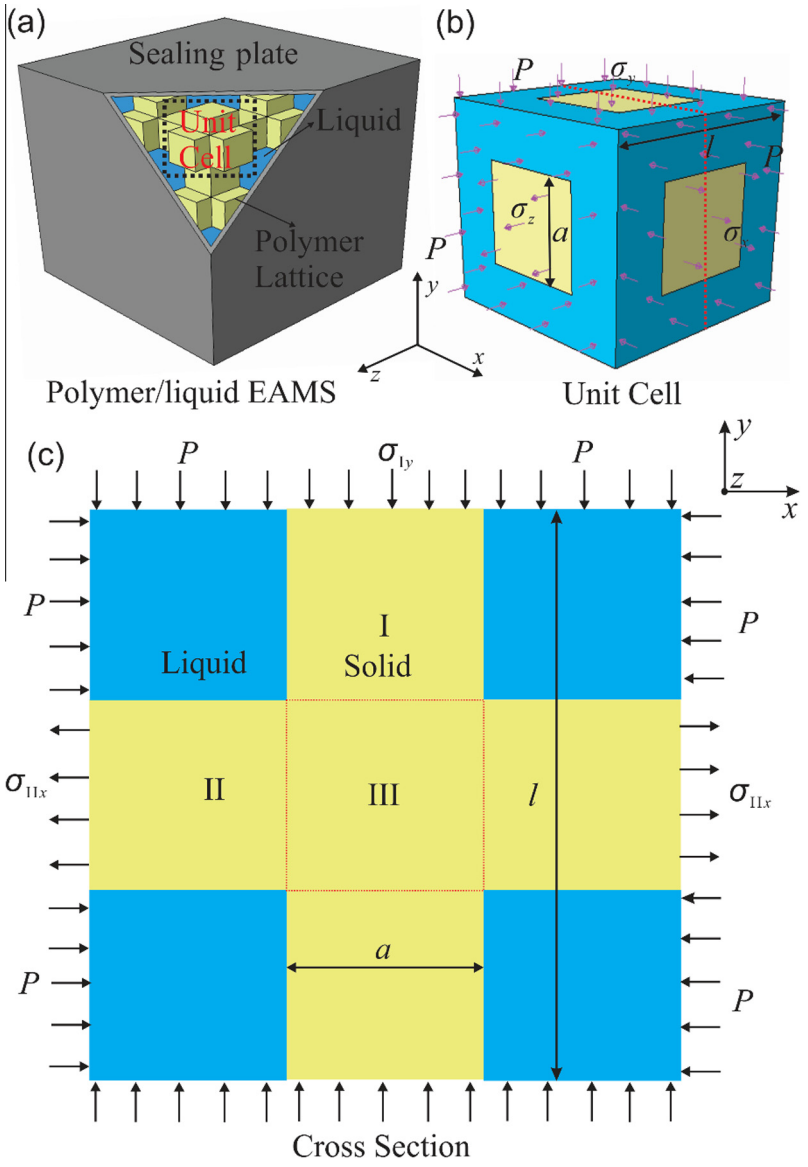

Fig. 1. Schematic illustrations of the co-continuous glassy polymer/liquid composite. (a) The energy absorption system of the co-continuous composites and (b) the unit cell of the polymer/liquid composites. (c) The cross section of the unit cell corresponding to red dashed line in (b). (For interpretation of the references to colour in this figure legend, the reader is referred to the web version of this article.)

The effective compressive strain of the unit cell in y direction ε_y is

$$\varepsilon_y = \left[\varepsilon_{1y}(l-a) + \varepsilon_{III y} a)\right]/l = \frac{\sigma_{1y}}{E} - \frac{P}{E}k_4, \tag{8}$$

where $k_4 = 2v(l/a - 1)$. Solving Eqs. (7) and (8) respecting to P and σ_{1y}, the pressure P can be rewritten as

$$P = -\frac{E\varepsilon_y k_1}{k_1 k_4 + k_2 + k_3 + \frac{E}{K}}. \tag{9}$$

Thus, the effective compressive stress of the unit cell with the liquid filler is

$$\begin{aligned}\sigma_{y,\mathrm{L}} &= (\sigma_{1y}A_{\mathrm{S}} - PA_{\mathrm{L}})/(A_{\mathrm{S}} + A_{\mathrm{L}}) \\ &= E\varepsilon_y\left[\frac{A_{\mathrm{S}}}{A_{\mathrm{S}} + A_{\mathrm{L}}} + \left(\frac{A_{\mathrm{L}}}{A_{\mathrm{S}} + A_{\mathrm{L}}} - \frac{A_{\mathrm{S}}}{A_{\mathrm{S}} + A_{\mathrm{L}}}k_4\right)\frac{k_1}{k_1 k_4 + k_2 + k_3 + \frac{E}{K}}\right].\end{aligned} \tag{10}$$

However, for the cross-shaped structure without the liquid filler the effective compress stress is

$$\sigma_{y,\mathrm{p}} = E\varepsilon_y \frac{A_{\mathrm{S}}}{A_{\mathrm{S}} + A_{\mathrm{L}}}, \tag{11}$$

which is equal to the first term in the right of Eq. (10). Hence, the second term of Eq. (10) is the enhancement of the liquid filler which comes from the additional support by liquid filler and lateral expansion of the porous solid structures. The stiffness, strength, as well as energy absorption are simultaneously improved. In the theoretical analysis we only consider the three dimensionally cross-shaped structure in the elastic deformation region. However, in practical applications the solid structure may be very complex. Besides, plastic yielding and buckling are usually occurred during compression, leading to very complicated compressive deformation, which is usually coupled with shear and bending deformation. Therefore it is hard to theoretically analyze the compressive deformation of such complex 3D composite structures. In the following sections

we will study the compressive mechanical behaviors of the co-continuous composites with triply periodic minimal surfaces through FEM simulations.

2.2. Simulation model of co-continuous composites with triply periodic minimal surfaces

The model systems of co-continuous glassy polymer/liquid composites studied here are based on microstructures which possess interfaces close to those of triply periodic minimal surfaces. These structures can provide better elastic properties compared to the rod-connected counterparts due to the effect of curvature in the ligaments [25]. Besides, based on our previous work the continuous interfaces are also beneficial to the load transfer between glassy polymer and rubbery polymer [12]. The stress concentration in glassy polymer is effectively suppressed and cracking behavior has not been observed under the compressive strain up to 25%. Here, three lattice structures (SC, FCC, and BCC) have been studied via finite element method.

Three types co-continuous structures with cubic symmetry are constructed based on the level set structures of triply periodic minimal surfaces. A level surface is defined by a function of the form $F:\mathbf{R}^3\rightarrow\mathbf{R}$ that satisfies the equation $F(x,y,z)=t$, where $t\in\mathbf{R}$ is a constant and $\{x,y,z\}\in\mathbf{R}^3$ are the coordinates of a point on the level surface. The level-set technique can be utilized to rapidly find suitable candidate functions that are invariant under the space group symmetry operations. The surface structures in Fig. 2 can be described by equations

$$\begin{aligned} f_{\mathrm{SC}}(x,y,z) &= \cos(x)+\cos(y)+\cos(z)-0.5\cos(x)\cos(y)\\ &\quad -0.5\cos(y)\cos(z)-0.5\cos(z)\cos(x)+t,\\ f_{\mathrm{BCC}}(x,y,z) &= \cos(x)\cos(y)+\cos(y)\cos(z)+\cos(z)\cos(x)+t,\\ f_{\mathrm{FCC}}(x,y,z) &= 4\cos(x)\cos(y)\cos(z)+\cos(2x)\cos(2y)\\ &\quad +\cos(2y)\cos(2z)+\cos(2z)\cos(2x)+t, \end{aligned} \tag{12}$$

where t is a constant that determines the volume fraction of the solid phase. As a result, the symmetry and volume distribution in these structures can be precisely controlled.

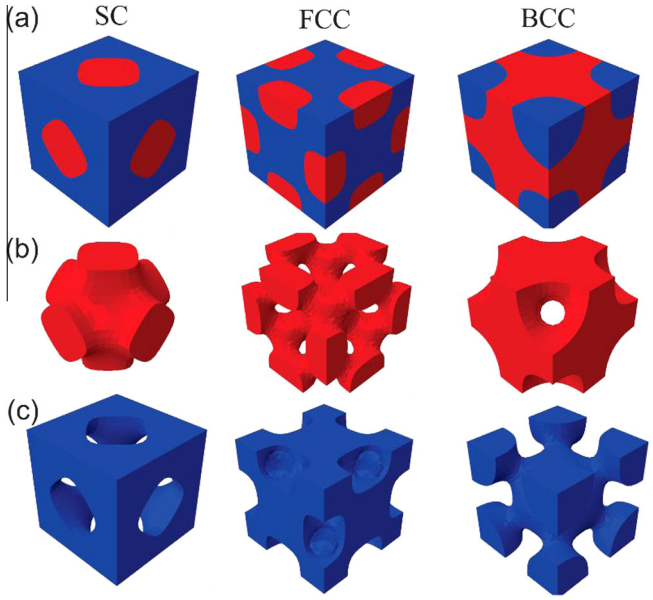

Fig. 2. (a) Unit cells of three lattice structures controlled by Eq. (1) with volume fraction 0.5, simple cubic (SC) lattice, face-centered-cubic (FCC) lattice, and body-centered-cubic (BCC) lattice. (b) The corresponding phase A and (c) the corresponding phase B.

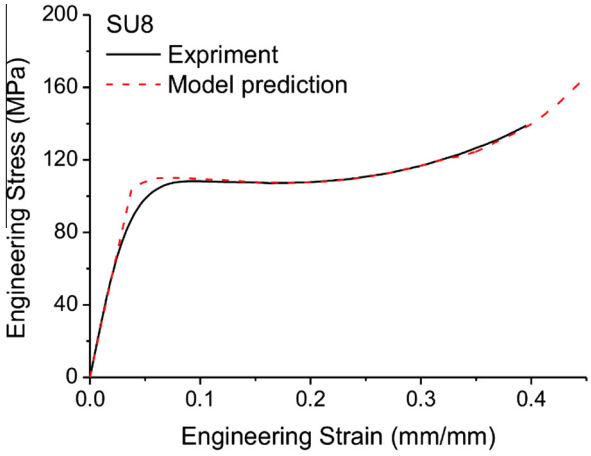

Fig. 3. The uniaxial tensile stress–strain curves of SU8 fiber in experiment (solid line) and FEM simulation (dashed line).

The glassy polymer in our model systems is taken from an epoxy, SU8, which is widely used in 3D micro- and nano-fabrication. The uniaxial tensile behaviors of SU8 fiber with diameter of 25 μm [12] are given in Fig. 3. Here, the stress–strain relation is linear for tensile strain smaller than 3%, which gives the elastic modulus of 2.9 GPa, and the Poisson ratio is set to 0.33 based on previous work [26]. In order to describe the plasticity and strain hardening effects of SU8, the isotropic hardening plasticity model is employed, where stress σ is represented by plastic strain ε_{p} as $\sigma=Y_0+E_{\mathrm{h}}\,e^{\varepsilon_{\mathrm{p}}/0.07}$. Here, Y_0=107 MPa is the yield strength and E_h = 2.7 MPa is the hardening modulus. Based on the elastic-isotropic hardening plasticity model, the uniaxial tensile behaviors of SU8 fiber are well depicted by FEM simulation, as seen the solid and dashed lines in Fig. 3. As in this work we only study the quasi-static compressive behaviors of co-continuous glassy polymer/liquid composites, the strain rate dependent mechanical properties of SU8 are not considered in our FEM simulation.

The liquid is described by equation of state (EOS) method in ABAQUS which is used in previous work to study the mechanical properties of microtruss/NMF liquid structures [16]. The relationship between the pressure P and the density ρ of liquid is

$$P=\frac{\rho_0 c_0^2\eta}{(1-s\eta)^2}\left(1-\frac{\Gamma_0\eta}{2}\right)+\Gamma_0\rho_0 E_m, \tag{13}$$

where ρ_0 is the reference density and ρ is the density of the liquid during compression, η is a state variable, defined as $\eta=1-\rho_0/\rho$, and $\rho_0c_0^2$ is equal to the bulk modulus of liquid at small strain. Here, in this work the liquid is assumed as water, that is $\rho_0c_0^2=2$ GPa. Currently, the EOS model in ABAQUS does not account for the macroscopic flow viscosity of liquid. However, for the present problem where the liquid is confined in porous SU8 structures, the macroscopic flow of liquid is negligible, so the flow viscosity has little influence on mechanical properties of the co-continuous glassy polymer/liquid composites.

3. FEM simulation results

The uniaxial compressive deformation of unit cells with SC, FCC, and BCC lattices is simulated via FEM simulations. The top surface of the unit cell is compressed vertically to the bottom surface with a constant strain rate of 0.01/s. Periodic boundary conditions are applied to lateral directions. For each lattice four kinds of material composition are considered, that are: phase A is SU8 and phase B is liquid (SU8-A/liquid-B), phase B is SU8 and phase A is liquid (SU8-B/liquid-A), phase A is SU8 and phase B is air (SU8-A), and

phase B is SU8 and phase A is air (SU8-B). For the co-continuous composites, a tie procedure is used to constrain the surfaces of liquid and solid, while for the porous structures the general contact procedure is employed to describe the self-contact of the porous structures. Both of SU8 and the liquid are described via C3D8R element and a mesh convergence study is carried out.

3.1. Quasi-static compressive behaviors

The dimensionless nominal stress and nominal strain curves are given in Fig. 4(a–c) for SC, FCC and BCC lattices, respectively. The volume fraction of phase A is 0.5 for the three structures. Here, the dimensionless nominal stress is defined as $F_y/AY_0\bar{\rho}$, where F_y is compressive force acting on the top surface of the unit cell during uniaxial compression, A is the cross sectional area of unit cell, Y_0 is the yield strength of SU8 and $\bar{\rho}$ is volume fraction of SU8. The nominal strain is defined as the ratio of the compressive displacement to the length of unit cell u_y/l. The unit cell length is $l = 6.28$ mm for all of the cases studied in this work.

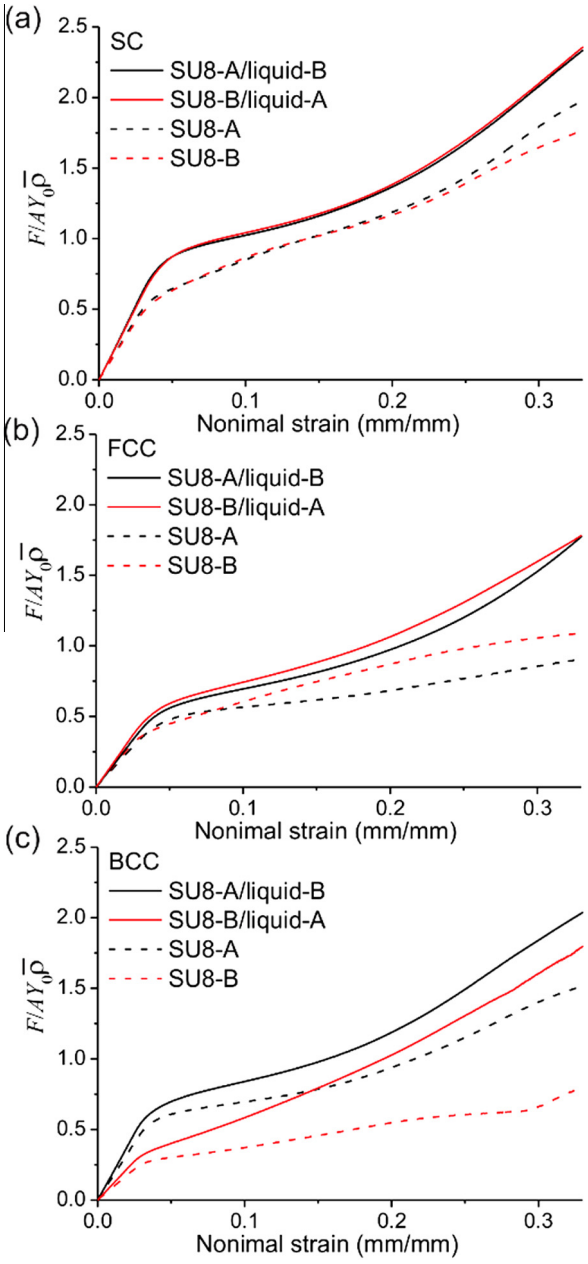

Fig. 4. The uniaxial compressive stress–strain curves for (a) SC, (b) FCC and (c) BCC lattices for two co-continuous composites SU8-A/liquid-B (black solid line), SU8-B/liquid-A (red solid line) and two porous structures SU8-A (black dashed line), SU8-B (red dashed line), respectively. The volume fraction of phase A is 0.5 for all three structures. (For interpretation of the references to color in this figure legend, the reader is referred to the web version of this article.)

The compressive stress–strain curves are linear at the beginning of compression followed by plastic yielding and plastic strain hardening for all of the lattices and material compositions studied here. Based on the stress–strain curves, effective elastic modulus and yield strength can be derived which will be discussed later. As shown in Fig. 4(a–c), because of the additional support of the liquid filler the effective stress of the co-continuous composites is always larger than their porous counterparts without liquid filler, so that the stiffness, strength and energy absorption are improved simultaneously. Besides, the yield strain of the co-continuous composites is also larger than that of the porous structures for all three lattices. This is because the stress distribution in SU8 ligaments of the co-continuous composites is more uniform than that of the porous structures and the stress concentration is effectively suppressed, so that the SU8 ligaments of co-continuous composites can endure higher compressive strain before yielding.

Here, the compressive deformation mechanism is different for different lattice structures. For SC lattice, the compressive deformation of phase A and phase B is mostly stretch-dominated and the effective stress–strain curves of SU8-A/liquid-B and SU8-B/liquid-A are almost identical, larger than that of the two porous structures (the effective stress–strain curves of the two porous structures are also almost the same). This is also due to the same volume fraction of phase A and phase B. For FCC lattice, the compressive deformation of phase A is more bending-dominated, so that the effective stress of SU8-A is smaller than that of SU8-B for both the co-continuous composites and the porous structures. In contrast, for BCC lattice the compressive deformation of phase B is more bending-dominated, so that the effective stress of SU8-B is smaller than that of SU8-A. This point is further verified by the von Mises stress distribution in Fig. 5 and the power indices of the relations of the effective elastic modulus, yield strength and energy absorption to the volume fraction of SU8 in Table 1.

The von Mises stress distribution in SU8 ligaments at nominal compressive strain 0.05 for the three lattices is given in Fig. 5. Here, the nominal compressive strain 0.05 is close to the yield point, as can be seen in Fig. 4. The von Mises stress distribution in the co-continuous composites is more uniform than that of the porous structures for SC, FCC, and BCC lattices. This is because the lateral expansion caused by the liquid filler will generate lateral stresses in lateral ligaments of the co-continuous composites. Therefore, the lateral SU8 ligaments of the co-continuous composites have higher stress than that of the porous structures, such as for SC lattice the stress in lateral ligaments of SU8-A/liquid-B and SU8-B/liquid-A is on the same level of the stress in vertical ligaments. But for the porous structures the stress in lateral ligaments is almost zero, as can be seen in Fig. 5. The similar phenomenon is also observed in FCC and BCC lattices. Therefore, more volume of SU8 is utilized to contribute to the load capacity and energy absorption, which is why the stiffness, strength, and energy absorption of the co-continuous composites are all enhanced as compared to that of the porous counterparts. Besides, from von Mises stress distribution we can also clarify the stretch-dominated and bending-dominated deformation behaviors, such as for SC lattice the main deformation is the compression of the vertical part, while for FCC lattice, such as SU8-A and SU8-A/liquid-B, and for BCC lattice, such as SU8-B and SU8-B/liquid-A, the main compressive deformation is the bending deformation of the interconnected ligaments, as can be seen in Fig. 5.

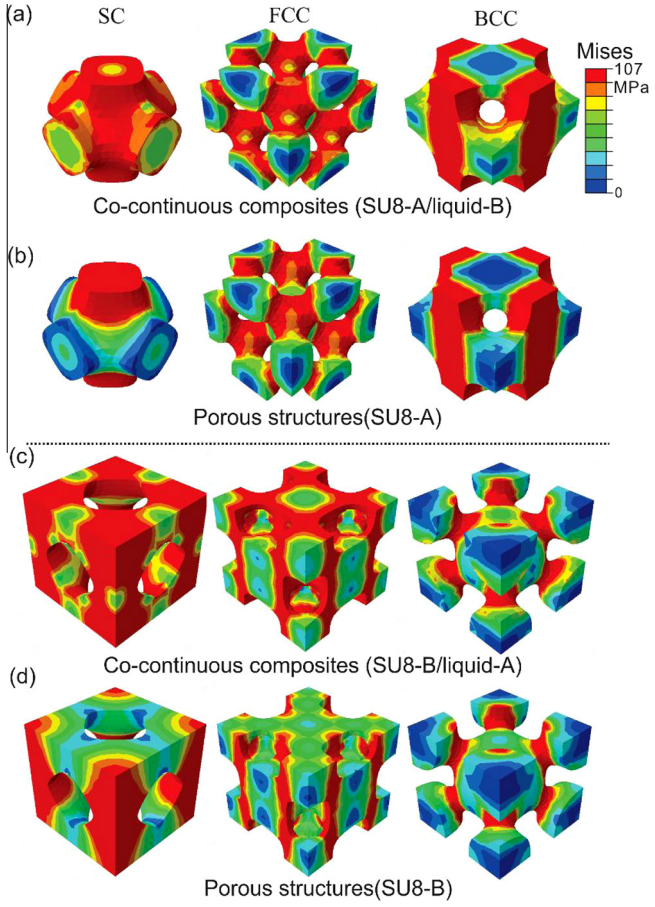

Fig. 5. von Mises stress distribution in the co-continuous composites and the porous structures at nominal compressive strain of 0.05. (a) von Mises stress distribution in co-continuous composites SU8-A/liquid-B for SC, FCC and BCC lattices and (b) the porous counterpart of SU8-A. (c) von Mises stress distribution in the co-continuous composites SU8-B/liquid-A and (d) the porous counterparts of SU8-B.

In Fig. 6 the lateral expansions for SC, FCC and BCC lattices during uniaxial compression are given. Due to liquid filler, the lateral expansion of the co-continuous composites is larger than their porous counterparts. For SC, FCC and BCC lattices, the lateral expansion of co-continuous composites ε_x and ε_z can be described by a uniform form

$$\varepsilon_x = \varepsilon_z = \frac{1}{\sqrt{1-\varepsilon_y}} - 1. \tag{14}$$

Furthermore, this relation is also valid for different volume fraction of SU8 from 0.25 to 0.6 studied in this work. The reason is that for co-continuous composites with liquid filler the volumetric deformation under uniaxial compression is negligible, especially in the post-yielding region. The volume of the unit cell after compression is $V = l^3(1-\varepsilon_y)(1+\varepsilon_z)(1+\varepsilon_x)$. Because the structures are symmetrical in x and z direction, the lateral expansion in x direction equals that in z direction, $\varepsilon_z = \varepsilon_x$. Then, if V is constant and we can obtain the lateral expansion $\varepsilon_x = \varepsilon_z = 1/(1-\varepsilon_y)^{0.5} - 1$, which describes very well the lateral expansion of co-continuous composites, see Fig. 6. However, for the porous structures, because of the voids in the structures there is volumetric deformation during uniaxial compression, so that the lateral expansion of porous structures is smaller than that of the co-continuous counterparts for SC, FCC,

Table 1
The relations of the effective elastic modulus, yield strength and energy absorption to the volume fraction of SU8 for the co-continuous glassy polymer/liquid composites.

Structures	Elastic modulus E/E_0		Yield strength Y/Y_0		Energy absorption U (MJ/m^3)	
	a	n	b	m	c(MJ/m^3)	η
SC (SU8-A/liquid-B)	0.92	1.2	0.93	1.1	31	1.1
SC (SU8-B/liquid-A)	0.98	1.4	0.97	1.2	33	1.2
FCC (SU8-A/liquid-B)	2.2	2.9	1.2	2.2	46	2.2
FCC (SU8-B/liquid-A)	1.0	1.9	1.0	2.0	34	1.8
BCC (SU8-A/liquid-B)	0.86	1.3	0.83	1.3	29	1.3
BCC (SU8-B/liquid-A)	1.5	3.1	1.5	3.4	46	2.6

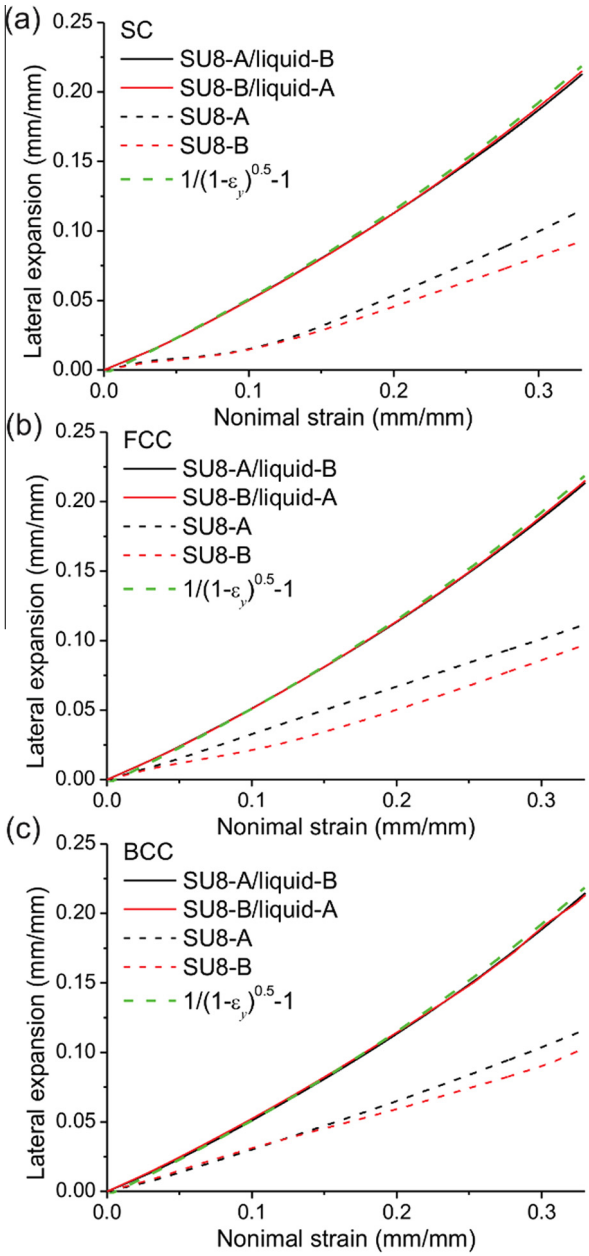

Fig. 6. The lateral expansion of SC, FCC, and BCC lattices during uniaxial compression. (a) The lateral expansion for SC lattice of SU8-A/liquid-B (black solid line), SU8-B/liquid-A (red solid line), SU8-A (black short dashed line) and SU8-B (red short dashed line), respectively. (b) The lateral expansion for FCC lattice and (c) The lateral expansion for BCC lattice. The green dashed line is Eq. (14). (For interpretation of the references to color in this figure legend, the reader is referred to the web version of this article.)

and BCC lattices. The lateral expansion of the porous structures is complex and depends on the lattice structures, as shown in Fig. 6. The lateral expansion further depends on the material composition, such as in Fig. 6(b) for FCC lattice the lateral expansion of SU8-A is larger than that of SU8-B.

3.2. Enhancement of the mechanical properties

In Fig. 7(a) the effective elastic modulus of the co-continuous composites for different volume fractions of phase A and different lattices of SC, FCC, and BCC is analyzed. Here, the effective elastic modulus is defined as the slope of the linear region of the stress–strain curves, as shown in Fig. 4(a–c). The effective elastic modulus increases as the volume fraction of phase A increases for material composition SU8-A/liquid-B. Otherwise it decreases for material composition SU8-B/liquid-A. It can be easily understood as the load is mainly carried by SU8, so that the composites with higher content of SU8 have higher stiffness. Generally, for the porous materials, such as metal foams and lattice structures, the relation between the effective elastic modulus E and relative density $\bar{\rho}$ can be described by a power law $E \sim \bar{\rho}^n$ [7,27,28]. Therefore, for the co-continuous composites with liquid filler we borrow this relation to describe the relation between the effective elastic modulus and the volume fraction of SU8 as $E/E_0 = a\bar{\rho}^n$. Here, as SU8 is the major load carrier, E_0 is Young's modulus of SU8 and $\bar{\rho}$ is volume fraction of SU8, a and n are two underdetermined parameters which can be obtained through fitting the FEM results. For SC, FCC, and BCC lattices, the two parameters are given in Table 1. The power index n equal to 1 indicates stretch-dominated deformation behavior such as axial compression of honeycombs and microtrusses, whereas power index n equal to 2 indicates bending-dominated deformation behavior such as metal and polymer foams [1,27–29]. For power index larger than 2 (usually found in aerogels and carbon nanotube foams) it means some parts in the materials are inefficient for load transfer [30,31]. The power index of the co-continuous composites ranges from 1.2 to 3.1, as shown in Table 1. The power index for SC lattice with material composition SU8-A/liquid-B is 1.2, so that the compressive deformation is almost stretch-dominated and the effective elastic modulus is the largest, see Fig. 7(a). In contrast, the power index for BCC lattice with material composition SU8-B/liquid-A is 3.1 (the largest) and the effective elastic modulus is the smallest. This is because for this type of structure the compressive deformation is the bending of the interconnected ligaments and a major part of the material does not contribute to the load carrier, see the von Mises stress distribution in Fig. 5. Therefore, a large volume of the material is insufficient to load transfer. The similar phenomenon is found for SU8-A/liquid-B of FCC lattice.

The ratio of the effective elastic modulus of the co-continuous composites to their porous counterparts is also studied, as shown in Fig. 7(b). It ranges from 1.1 to 1.3 as the volume fraction of phase A changes from 0.25 to 0.6 for all the co-continuous composites studied in this work. For SU8-A/liquid-B, the relative enhancement decreases as the volume fraction of phase A increases, and for SU8-B/liquid-A it increases which is opposite to the relations of the effective elastic modulus to the volume fraction of phase A, as compared in Fig. 7(a) and (b). This is because the relative enhancement originates from the additional support of the liquid filler, so that the higher content of liquid filler has larger relative enhancement. However, the relative enhancement of SU8-A/liquid-B for FCC lattice at the volume fraction of 0.54 is larger than the values at the volume fraction of 0.5 and 0.33. This is because the deformation of FCC lattice is very complex which combines with bending-dominated deformation and insufficient load transfer (the power index is 2.9). The liquid filler may suppress the insufficient load transfer so as to increase the relative enhancement at the volume fraction of 0.54.

The yield strength and the energy absorption for different volume fractions of phase A are also studied and shown in Fig. 7(c–f). Here, the energy absorption is defined as the area enclosed by the stress–strain curves at the compressive strain of 25%. The reason of selecting 25% compressive strain is that based on the previous work, the co-continuous composites and porous structures are intact at the compressive strain [12]. In this work, we do not intend to study the fracture process. Similar to the effective elastic modulus, the yield strength and the energy absorption increase as the volume fraction of phase A increases for SU8-A/liquid-B and they decreases for SU8-B/liquid-A. Besides, the co-continuous composites whose deformation is stretch-dominated, such as SC lattice, have higher yield strength and energy absorption, while the co-continuous composites whose deformation is bending-dominated, such as SU8-B/liquid-A of BCC lattice, have lower yield strength and energy absorption. It is also consisted with the behaviors of the effective elastic modulus. The relations of the yield strength and the energy absorption to the volume fraction of SU8 can also be described by power laws which are $Y/Y_0 = b\bar{\rho}^m$ for yield strength and $U = c\bar{\rho}^\eta$ for energy absorption, where Y_0 is yield strength of SU8. The underdetermined parameters b, m and c, η can be obtained by fitting to the simulation results. From Table 1 we can see the power indices of the effective elastic modulus, yield strength, and energy absorption are almost the same for the same structure which means the effective elastic modulus, yield strength and energy absorption are mostly determined by the deformation mechanism resulting from the composite geometry.

The ratios of the yield strength and the energy absorption for the co-continuous composites to their porous counterparts are also analyzed. The relative enhancement of the yield strength and the energy absorption ranges from 1.1 to 2.3 compared to 1.1 to 1.35 for effective elastic modulus. Therefore, the liquid filler is more efficient to improve yield strength and energy absorption of the co-continuous composites. This is because the yield strength and energy absorption are significantly influenced by the local plastic yielding of the glassy polymer and the liquid filler can effectively suppress the local deformation of the glassy polymer, so that it is more efficient to improve the yield strength and energy absorption of the co-continuous composites. For the yield strength, the SC lattice (stretch-dominated deformation) has larger relative enhancement, see Fig. 7(d). But for energy absorption, the co-continuous composites with bending-dominated deformation, such as SU8-B/liquid-A for BCC lattice, have larger relative enhancement, see Fig. 7(f).

The liquid filler can increase the stiffness, yield strength and energy absorption of the co-continuous composites, but the cost is to increase the mass of EAMS. Therefore, we have compared the specific elastic modulus E/ρ of the porous structures and the co-continuous composites studied in this work, and also other porous materials reported in previous literature [1,29,30,32], as shown in Fig. 8(a). Generally, the specific elastic modulus of the co-continuous polymer/liquid composites is on the same order of the porous structures. But due to the liquid filler, the density of the co-continuous composites is larger than the porous structures. The benefit is the density of the co-continuous composites is almost constant and one can tune the mechanical properties of the co-continuous composites with their density unvaried. Compared to other porous materials reported in previous literature, the specific elastic modulus of the co-continuous composites is also among the top values [1,29,30,32]. One should be noted the porous materials with high specific elastic modulus, such as solid Al_2O_3 lattice and hollow Al_2O_3 lattice, are usually brittle [32], while the co-continuous composites have very good compressibility and

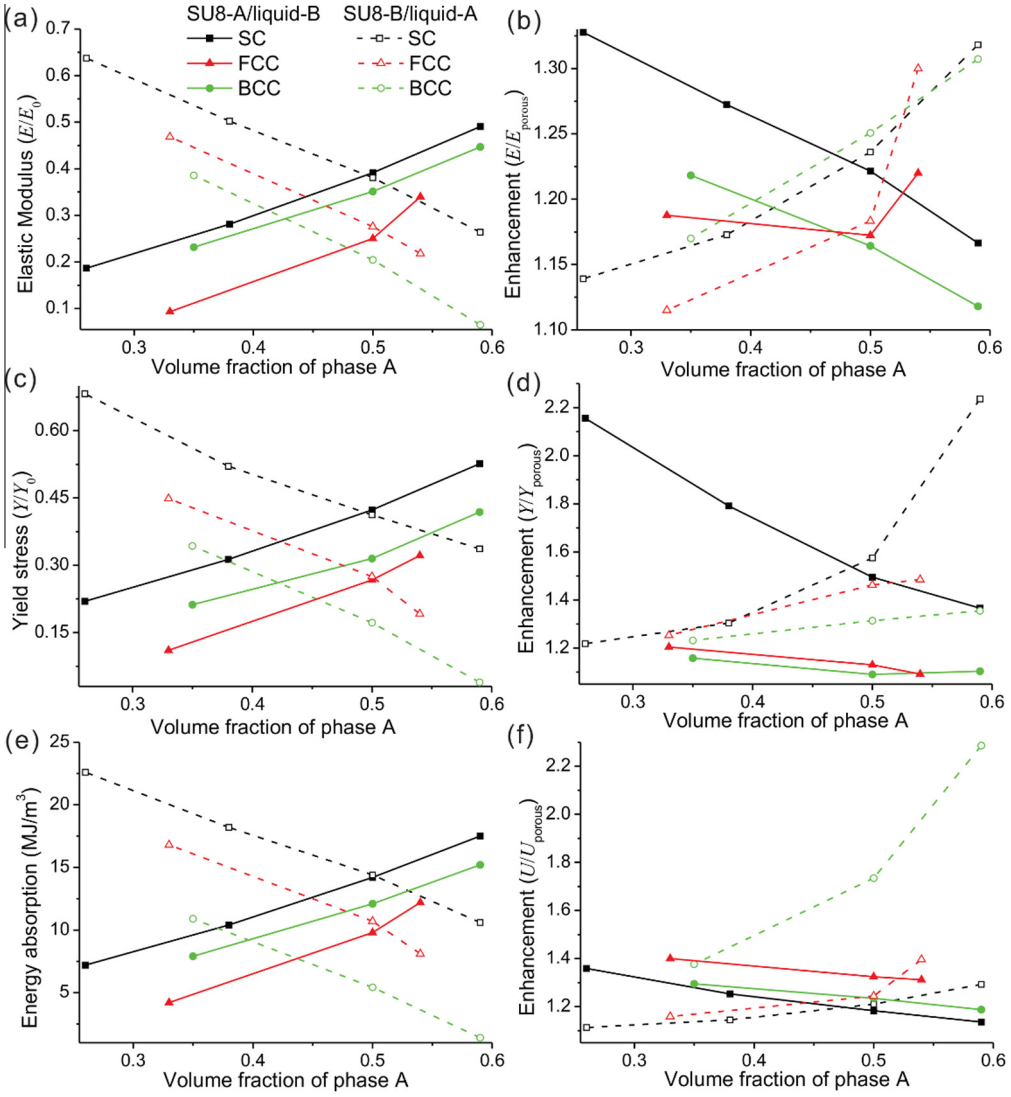

Fig. 7. The relations of the effective elastic modulus, yield strength, and energy absorption to the volume fraction of phase A for SC, FCC, and BCC lattices and the relative enhancement to their porous counterparts. (a) The relations between effective elastic modulus of co-continuous composites and volume fraction of phase A for SC, FCC, and BCC lattices. The material composition SU8-A/liquid-B is represented by solid symbols and SU8-B/liquid-A is represented by open symbols. (b) The relative enhancement of effective elastic modulus of the co-continuous composites to their porous counterparts. (c, d) The relations of yield strength and the relative enhancement to volume fraction of phase A. (e, f) The relations of energy absorption and the relative enhancement to the volume fraction of phase A.

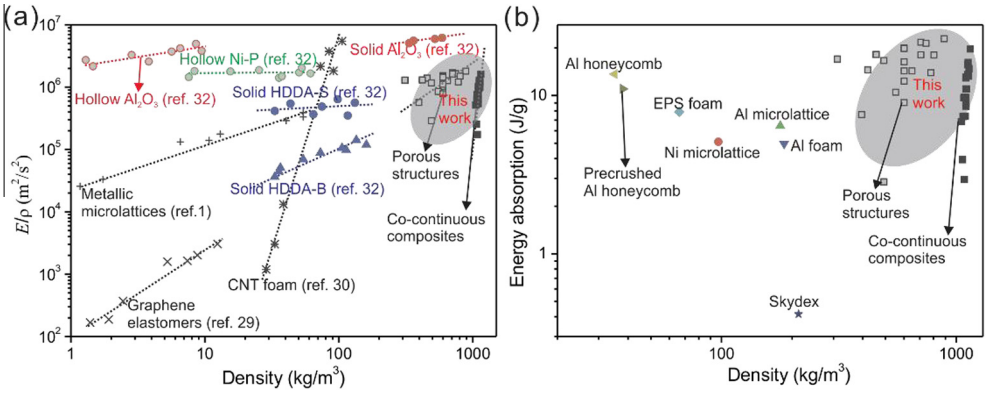

Fig. 8. (a) The specific elastic modulus of the co-continuous composites, the porous structures, and other porous materials reported in previous literature [1,29,30,32]. (b) The energy absorption per mass of the co-continuous composites, the porous structures, and other porous materials reported in Ref. [33].

energy absorption. The similar relation is also found for the energy absorption per mass of the co-continuous composites and the porous structures, see also Fig. 8(b). Compared to the other previously studied materials, the co-continuous composites have very good energy absorption capability [33]. Besides, the functional fillers (e.g. NMF liquid, phase-change materials, dielectric elastomer, etc.) can further bring multifunctionality to the protective structures, which hold great potential applications in desert body armor, smart structures, and energy harvesting structures, etc [16,18,34].

4. Discussions

In practical applications, the co-continuous glassy polymer/liquid composites should be sealed to achieve the enhancement of the liquid filler. For example, the co-continuous composites can be sandwiched by two face panels. Then, the external impulse energy can be absorbed by the co-continuous composites and face panels [3,35]. Here, the possible failure mechanisms of the co-continuous composites are fracture of the glassy polymer structures and leaking of the liquid filler. For glassy polymer SU8, its tensile strain at fracture is larger than 0.4, as shown in Fig. 3. Therefore, it is very suitable to construct the solid frameworks of the co-continuous composites and the optimal design of proper arrangements of SU8 constituents to avoid large stress concentration during compression. One of the possible routines is to construct the co-continuous composites based on the level set structures of triply periodic minimal surfaces. Previous experimental work has shown the cubic symmetrical lattice structures (e.g. SC, FCC, BCC) can endure compressive strain up to 0.25 without cracking [12]. Besides, the liquid filler is also beneficial to decrease the stress concentration in the co-continuous composites. In the future work, more geometrical and topological structures should be tested to combine the deformation of plastic yielding, plastic buckling, and elastic buckling to achieve higher compressibility of the co-continuous composites.

The sealing is another challenge problem for the co-continuous glassy polymer/liquid composites. If leaking occurs, the enhancement by the liquid filler is weakened or even vanished. In order to maintain the integrity of the sealing during compression, three requirements are needed: (1) the sealing should have enough strength to constrain the liquid in the co-continuous composites during compression, (2) the deformation of the sealing should be compatible with the co-continuous composites and the outside structures, such as the face panels of the sandwich beam, (3) in addition, the sealing should better be robust which means the failure of the sealing at one point does not influence the whole co-continuous composites. One of the possible solutions is modular sealing with rubbery polymer. The co-continuous composites can be divided into relative small cells and every cell is sealed separately with rubbery polymer, and then the encapsulated cells are assembled into the protective structures. Here, the rubbery polymer sealing can be fabricated through 3D printing which shows very good interface strength [12]. The rubbery polymer is also flexible and can deform compatibly with the co-continuous composites and the outside structures. Besides, due to the modular sealing the failure of one cell does not cause the catastrophic failure of the whole co-continuous composites.

In this work we have only studied the quasi-static compressive behaviors of the co-continuous glassy polymer/liquid composites. Indeed, the dynamic effects (e.g. micro-inertial effect, shock wave effect, and strain rate effect of the materials) have very significantly influence to the mechanical behaviors of protective structures [5]. Especially for the glassy polymer SU8, its yield strength significantly increases as strain rate increases. Besides, the leaking of liquid filler is also suppressed at dynamic loads. In the future work, the dynamic effects of the co-continuous composites will be systematically studied.

5. Conclusions

In summary, we have investigated the compressive behaviors of co-continuous glassy polymer/liquid composites with different geometric arrangements of SC, FCC, and BCC lattices. We have shown that the effective stiffness, yield strength and energy absorption of the co-continuous composites can be enhanced simultaneously by the liquid filler. The enhancement originates from the additional support of the liquid filler and the lateral expansion of the glassy polymer structures. The stress distribution is more uniform in the co-continuous composites. Hence, more materials contribute to the load capacity and energy absorption. The compression of SC lattice structure is stretch-dominated, which has the highest stiffness, yield strength and energy absorption, while the compression of SU8-B/liquid-A for BCC lattice is more bending-dominated, which has the lowest stiffness, yield strength and energy absorption. A general power law can be used to describe the relations of the effective elastic modulus, yield strength and energy absorption to the volume fraction of SU8. The power indices of the three characteristics are almost identical for the same structure. These results provide guidelines for engineering and tailoring the nonlinear mechanical behaviors and energy absorption of co-continuous composites for a wide range of applications and further creating multifunctional materials. For example, polymeric materials and/or liquid filler, which can change shape, volume and material properties in response to external stimuli such as a temperature or electric field, can provide additional functionality when used as one of the phases. While the feature lengthscale of current study is at millimeter scale, these results can extend down to micron or sub-micron lengthscale where fabrication challenges can be met with innovative lithography and other processing techniques such as block copolymer for periodic structures [13,36–38]. At these smaller scales, further property enhancement may result due to lengthscale effect on, for example, strength and ductility [26,39–41]. Ongoing and future research addresses the study of multifunctionality, smart structures, as well as wave propagation and vibration control.

Acknowledgments

The authors acknowledge financial support from the National Natural Science Foundation of China (11302163 and 11321062) and the National Science Foundation under Award number CMMI-1437449.

References

[1] Schaedler TA, Jacobsen AJ, Torrents A, Sorensen AE, Lian J, Greer JR, et al. Ultralight metallic microlattices. Science 2011;334:962–5.
[2] Qin QH, Wang T. An analytical solution for the large deflections of a slender sandwich beam with a metallic foam core under transverse loading by a flat punch. Compos Struct 2009;88:509–18.
[3] Xiong J, Ma L, Stocchi A, Yang J, Wu L, Pan S. Bending response of carbon fiber composite sandwich beams with three dimensional honeycomb cores. Compos Struct 2014;108:234–42.
[4] Meza LR, Das S, Greer JR. Strong, lightweight, and recoverable three-dimensional ceramic nanolattices. Science 2014;345:1322–6.
[5] Liu Y, Schaedler TA, Chen X. Dynamic energy absorption characteristics of hollow microlattice structures. Mech Mater 2014;77:1–13.
[6] Jang D, Meza LR, Greer F, Greer JR. Fabrication and deformation of three-dimensional hollow ceramic nanostructures. Nat Mater 2013;12:893–8.
[7] Gibson LJ, Ashby MF. Cellular solids: structure and properties. New York: Cambridge University Press; 1997.
[8] Novak BM. Hybrid nanocomposite materials-between inorganic glasses and organic polymers. Adv Mater 1993;5:422–33.

[9] Ji B, Gao H. Mechanical properties of nanostructure of biological materials. J Mech Phys Solids 2004;52:1963–90.
[10] Wang L, Boyce MC. Bioinspired structural material exhibiting post-yield lateral expansion and volumetric energy dissipation during tension. Adv Funct Mater 2010;20:3025–30.
[11] Liu Y, Xu Z. Multimodal and self-healable Interfaces enable strong and tough graphene-derived materials. J Mech Phys Solids 2014;70:30–41.
[12] Wang L, Lau J, Thomas EL, Boyce MC. Co-continuous composite materials for stiffness, strength, and energy dissipation. Adv Mater 2011;23:1524–9.
[13] Thomas EL, Anderson DM, Henkee CS, Hoffman D. Periodic area-minimizing surfaces in block copolymers. Nature 1988;334:598–601.
[14] Han A, Punyamurtula VK, Kim T, Qiao Y. The upper limit of energy density of nanoporous materials functionalized liquid. J Mater Eng Perform 2008;17:326–9.
[15] Surani FB, Kong XG, Panchal DB, Qiao Y. Energy absorption of a nanoporous system subjected to dynamic loadings. Appl Phys Lett 2005;87:163111.
[16] Liu Y, Schaedler TA, Jacobsen AJ, Lu W, Qiao Y, Chen X. Quasi-static crush behavior of hollow microtruss filled with NMF liquid. Compos Struct 2014;115:29–40.
[17] Flouris A, Cheung S. Design and control optimization of microclimate liquid cooling systems underneath protective clothing. Ann Biomed Eng 2006;34:359–72.
[18] Larsen B, Netto K, Aisbett B. The effect of body armor on performance, thermal stress, and exertion: a critical review. Mil Med 2011;176:1265–73.
[19] Kiekens P, Jayaraman S. Intelligent textiles and clothing for ballistic and NBC protection. Springer; 2012.
[20] Ziherl P, Kamien RD. Soap froths and crystal structures. Phys Rev Lett 2000;85:3528.
[21] Lu Y, Yang Y, Sellinger A, Lu M, Huang J, Fan H, et al. Self-assembly of mesoscopically ordered chromatic polydiacetylene/silica nanocomposites. Nature 2001;410:913–7.
[22] Ha YH, Vaia RA, Lynn WF, Costantino JP, Shin J, Smith AB, et al. Three-dimensional network photonic crystals via cyclic size reduction/infiltration of sea urchin exoskeleton. Adv Mater 2004;16:1091–4.
[23] Torquato S, Hyun S, Donev A. Multifunctional composites: optimizing microstructures for simultaneous transport of heat and electricity. Phys Rev Lett 2002;89:266601.
[24] Torquato S, Donev A. Minimal surfaces and multifunctionality. Proc R Soc London Ser A: Math Phys Eng Sci 2004;460:1849–56.
[25] Maldovan M, Ullal CK, Jang JH, Thomas EL. Sub-micrometer scale periodic porous cellular structures: microframes prepared by holographic interference lithography. Adv Mater 2007;19:3809–13.
[26] Wang L, Boyce MC, Wen CY, Thomas EL. Plastic dissipation mechanisms in periodic microframe-structured polymers. Adv Funct Mater 2009;19:1343–50.
[27] Ashby MF. The properties of foams and lattices. Philos Trans R Soc A-Math Phys Eng Sci 2006;364:15–30.
[28] Liu Y, Schaedler TA, Jacobsen AJ, Chen X. Quasi-static energy absorption of hollow microlattice structures. Composites Part B: Eng 2014;67:39–49.
[29] Qiu L, Liu JZ, Chang SL, Wu Y, Li D. Biomimetic superelastic graphene-based cellular monoliths. Nat Commun 2012;3:1241.
[30] Worsley MA, Kucheyev SO, Satcher Jr JH, Hamza AV, Baumann TF. Mechanically robust and electrically conductive carbon nanotube foams. Appl Phys Lett 2009;94:073115.
[31] Moner-Girona M, Roig A, Molins E, Martınez E, Esteve J. Micromechanical properties of silica aerogels. Appl Phys Lett 1999;75:653–5.
[32] Zheng X, Lee H, Weisgraber TH, Shusteff M, DeOtte J, Duoss EB, et al. Ultralight, ultrastiff mechanical metamaterials. Science 2014;344:1373–7.
[33] Schaedler TA, Ro CJ, Sorensen AE, Eckel Z, Yang SS, Carter WB, et al. Designing metallic microlattices for energy absorber applications. Adv Eng Mater 2014;16:276–83.
[34] Kornbluh RD, Pelrine R, Prahlad H, Wong-Foy A, McCoy B, Kim S, et al. From boots to buoys: promises and challenges of dielectric elastomer energy harvesting. SPIE smart structures and materials nondestructive evaluation and health monitoring: international society for optics and photonics 2011:797605.
[35] Wang Z, Jing L, Ning J, Zhao L. The structural response of clamped sandwich beams subjected to impact loading. Compos Struct 2011;93:1300–8.
[36] Maldovan M, Thomas EL. Periodic materials and interference lithography: for photonics, phononics and mechanics. John Wiley & Sons; 2009.
[37] Dair BJ, Honeker CC, Alward DB, Avgeropoulos A, Hadjichristidis N, Fetters LJ, et al. Mechanical properties and deformation behavior of the double gyroid phase in unoriented thermoplastic elastomers. Macromolecules 1999;32:8145–52.
[38] Lee J-H, Wang L, Boyce MC, Thomas EL. Periodic bicontinuous composites for high specific energy absorption. Nano Lett 2012;12:4392–6.
[39] Jang J-H, Ullal CK, Gorishnyy T, Tsukruk VV, Thomas EL. Mechanically tunable three-dimensional elastomeric network/air structures via interference lithography. Nano Lett 2006;6:740–3.
[40] Jang JH, Ullal CK, Choi T, Lemieux MC, Tsukruk VV, Thomas EL. 3D polymer microframes that exploit length-scale-dependent mechanical behavior. Adv Mater 2006;18:2123–7.
[41] Lee J-H, Wang L, Kooi S, Boyce MC, Thomas EL. Enhanced energy dissipation in periodic epoxy nanoframes. Nano Lett 2010;10:2592–7.